

RSC Advances



This is an *Accepted Manuscript*, which has been through the Royal Society of Chemistry peer review process and has been accepted for publication.

Accepted Manuscripts are published online shortly after acceptance, before technical editing, formatting and proof reading. Using this free service, authors can make their results available to the community, in citable form, before we publish the edited article. This *Accepted Manuscript* will be replaced by the edited, formatted and paginated article as soon as this is available.

You can find more information about *Accepted Manuscripts* in the [Information for Authors](#).

Please note that technical editing may introduce minor changes to the text and/or graphics, which may alter content. The journal's standard [Terms & Conditions](#) and the [Ethical guidelines](#) still apply. In no event shall the Royal Society of Chemistry be held responsible for any errors or omissions in this *Accepted Manuscript* or any consequences arising from the use of any information it contains.

A Bead-Based Microfluidic Approach to Integrated Single-Cell Gene Expression Analysis by Quantitative RT-PCR

Hao Sun^{a,b}, Tim Olsen^b, Jing Zhu^b, Jianguo Tao^a, Brian Ponnaiya^c, Sally A. Amundson^d, David J. Brenner^{c,d}, and Qiao Lin^{*b}

^aDepartment of Mechatronics Engineering, Harbin Institute of Technology, Harbin, Heilongjiang, China, ^bDepartment of Mechanical Engineering, ^cCenter for Radiological Research, and ^dDepartment of Radiation Oncology, Columbia University, New York, NY, USA

*Corresponding author.

E-mail address: qlin@columbia.edu (Q. Lin)

Abstract Gene expression analysis at the single-cell level is critical to understanding variations among cells in heterogeneous populations. Microfluidic reverse transcription quantitative real-time polymerase chain reaction (RT-qPCR) is well suited to gene expression assays of single cells. We present a microfluidic approach that integrate all functional steps for RT-qPCR of a single cell, including isolation and lysis of the cell, as well as purification, reverse transcription and quantitative real-time PCR of messenger RNA in the cell lysate. In this approach, all reactions in the multi-step assay of a single lysed cell can be completed on microbeads, thereby simplifying the design, fabrication and operation of the microfluidic device, as well as facilitating the minimization of sample loss or contamination. In the microfluidic device, a single cell is isolated and lysed; mRNA in the cell lysate is then analyzed by RT-qPCR using primers immobilized on microbeads in a single microchamber whose temperature is controlled in closed loop via an integrated heater and temperature sensor. The utility of the approach was demonstrated by the analysis of the effects of the drug (methyl methanesulfonate, MMS) on the induction of the cyclin-dependent kinase inhibitor 1a (CDKN1A) in single human cancer cells (MCF-7), demonstrating the potential of our approach for efficient, integrated single-cell RT-qPCR for gene expression analysis.

Keywords: Single cell analysis, Microfluidic, Microbead, RT-qPCR

1. Introduction

A major challenge in gene expression profiling is the ubiquitous heterogeneity existing in biological samples^{1,2}. Conventionally, gene expression measurements are focused on groups of cells from organs, tissues or cell culture as the measurement technologies have been limited by accuracy, sensitivity, and dynamic range. While cells may appear morphologically identical, recent evidence reveals that gene expression level of individual cells in a population can vary due to cellular heterogeneity³. Thus, gene expression studies using groups of cells can fail to detect differences in the molecular composition of individual cells^{1,4}.

Single-cell gene expression profiling, a method to assay the gene patterns in individual cells, is capable of alleviating the complexity of genetic variability caused by heterogeneity and has the potential to reveal intracellular molecular mechanisms and pathways⁵. For example, environmental stimuli lead to variations in expression which can be manifested at the level of single-cell gene regulatory networks⁶. By quantifying the alterations in gene expression, the influence of the stimuli on genes can be identified. Most recently, by combining next-generation nucleic acid sequencing with improved biochemical methodologies such as template switching technology (Smart-seq)⁷, transcriptome *in vivo* analysis (TIVA)⁸, unique molecular identifiers (UMIs)⁹ and fluorescent *in situ* RNA sequencing (FISSEQ)¹⁰, genetic analysis at the single cell or single molecule level has been used in applications such as personalizing therapy¹¹, drug discovery¹² and embryonic stem cell research¹³. However, such assays have been technically challenging due to the low quantity and degradation of RNA from an individual cell¹⁴⁻¹⁶. A typical mammalian cell contains about 10-30 pg of RNA of which 1-5%, depending on cell type and physiological state, is mRNA corresponding to 10^5 - 10^6 molecules¹⁷.

Microfluidic technology is capable of rapid, sensitive and quantitative assays in small sample volumes while eliminating the need for labor intensive and potentially error-prone laboratory manipulation¹⁸. Much effort has been devoted to developing single-cell gene expression profiling analysis in microfluidics¹⁹⁻²⁵. Microchip-based fluorescence in situ hybridization (FISH) has been used to detect and localize the presence or absence of specific DNA sequences²⁶. Microchips have also been combined with emulsion reverse transcription polymerase chain reaction (eRT-PCR) by employing the thermoresponsive sol-gel switching properties of agarose. In comparison, microfluidic quantitative reverse transcription polymerase chain reaction (RT-qPCR), which detects gene expression through the creation of complementary DNA (cDNA) transcripts from RNA offers large dynamic ranges as well as high sensitivity and accuracy^{27, 28}. For example, a microfluidic device for gene expression measurements was developed employing an open-loop infrared laser-based thermal control system where RNA templates from the lysate of cells can be quantitatively analyzed²⁹. A microchip has also been presented to capture single cells and reverse transcribe messenger RNA (mRNA) in cell lysate to cDNA, which is fed into a commercial system (BioMark, Fluidigm) for analysis³⁰. While representing significant progress towards single-cell gene expression profiling, these approaches require off-chip manual transfer of RNA (which is a common source of potential contamination to the samples), rely on off-chip thermal control instrumentation, or involve rather complicated flow control components and operations.

We present an approach that, in contrast to existing microfluidic RT-qPCR methods, realizes complete microfluidic integration of single-cell RT-qPCR. This approach integrates isolation, immobilization and lysis of single cells with microbead-based purification, reverse transcription (RT) and quantitative real-time

PCR (qPCR) of mRNA in the cell lysate, without requiring off-chip manual transfer of cells and reagents between the individual reaction steps, and without using off-chip qPCR instruments. Furthermore, our approach affords implementation in a device that is simple in design, fabrication and operation. As such, the approach offers a high level of efficiency, allows minimization of loss or cross contamination of analytes (which is particularly significant for low mRNA abundance in the case of single cells), and is amenable to parallelized and multiplexed gene expression analysis. The utility of our approach for potentially enabling rapid, sensitive and reliable single-cell gene expression analysis is demonstrated by analysis of the effects of the drug (methyl methanesulfonate, MMS) on the induction of the cyclin-dependent kinase inhibitor 1a (CDKN1A) in single cells of the MCF-7 breast cancer cell line.

2. Principle, Design and Experimental

2.1 Principle

The device is capable of cell-trapping, cell lysis and bead-based RT-qPCR. Hydrodynamic forces were employed for efficient and reliable isolation and immobilization of single cells, which is important to downstream quantitative single-cell genetic analysis including cell lysis, mRNA purification, reverse transcription and DNA duplication. Once immobilized, single cells were lysed chemically and mRNA templates from the lysate were captured using microbeads. The principle of mRNA capture relies on base pairing between the polyA tails of the mRNA and the oligo(dT)₂₅ residues covalently coupled to the surface of the beads. For reverse transcription (RT) the bead-bound oligo(dT)₂₅ functions as a primer for the synthesis of cDNA. After RT, the synthesized cDNA templates were amplified while the accumulation of products was real-time quantified using a hydrolysis

probe/primer set (TaqMan®) (Fig. 1A). The reagent probe/primer consists of a fluorescein amidite (FAM) reporter dye, a minor groove binder (MGB) and a nonfluorescent quencher (NFQ). When the probe is intact, by the Förster resonance energy transfer³¹, the reporter fluorescence is suppressed by the quencher. During a PCR annealing process, the probe will bind to a complementary region of the target template. The quencher will be cleaved from the probe during the subsequent elongation process causing fluorescence of the reporter dye to increase. In addition, to correct for fluorescent fluctuations due to batch-to-batch changes in cavity volume and PCR component concentrations, a passive reference (ROX) was employed to normalize the FAM signal during real-time measurements. Fluorescent images of the beads were taken in two different colors (ROX and FAM) after each PCR cycle. Furthermore, the approach was applied to gene regulation studies by treating cells with MMS to detect drug induced single cell gene expression level alterations.

2.2 Design

The device consists of a temperature control chip with an integrated heater and temperature sensor, and a polydimethylsiloxane (PDMS) microchamber and a cell trapping unit (Fig. 1B). First, a single elliptically shaped reaction chamber (7.7 mm in length, 5.7 mm in width, 15 μm in height and 658 ± 25 nL in volume) was designed for the two-step RT-qPCR process. The cell trapping unit consists of a neck-shaped channel (800 μm in length, 100 μm in width and 15 μm in height) with a protruding structure that reduces the channel width from 100 μm to 5 μm . The cell trapping unit was also equipped with a cell carrier flow outlet, a cell washing outlet and two pneumatic control channels (600 μm in length, 400 μm in width and 80 μm in height) to divert flow for cell trapping, and lysis. A serpentine-shaped temperature sensor

(linewidth: 50 μm) and heater (linewidth: 400 μm) were integrated beneath the center of the reaction chamber. In addition, to inhibit reagent evaporation and diffusion caused by PDMS porosity, a transparent and pressure-sensitive adhesive film (3 mm in length and 0.5 mm in width) was bonded on top of the reaction chamber.

2.3 Experimental Procedure

Prior to each on-chip test, the device was incubated with 1 mg/mL BSA solution in PBS at room temperature for at least 30 min to prevent small molecule absorption into the PDMS surface. Before introduction into the device, beads were washed using binding buffer (20 mM Tris-HCl, pH 7.5, 1.0 M LiCl, 2 mM EDTA) from the Dynabeads® mRNA Kit and resuspended in a vial, and then were transferred to an RNase-free tube. The tube was placed over a magnet for 1 min, the supernatant was discarded and the binding buffer was added to resuspend the beads. Following the final supernatant removal, the beads were suspended in 2 μL binding buffer (approximately 7.5×10^6) and introduced to the device using a microcapillary pipette. The beads entering the chamber were retained by an external magnetic placed underneath the chip, and the approximate number of beads was determined by analysis of the microscope image using ImageJ.

MCF-7 cells were incubated with MEM media supplemented with 10% FBS and 1% P/S, and were kept at 37 °C in a humidified incubator containing 5% CO₂. Cells used in these experiments, which compared MMS modified cells with non-MMS modified cells, were from the same generation of MCF-7 cells to eliminate potential generational gene expression differences. Before each experiment, cells were collected through centrifugation resuspended at 10^8 cells/mL in MEM and then kept on ice. During the experiments, MCF-7 cell suspension was first diluted to 10^5 cells/mL in a

microcentrifuge tube, and mixed to homogenize the suspension and break up cell clusters. The homogenized cell suspension was then driven into the device *via* a syringe pump while valves were used to manipulate the direction of the flow. The trapping structure was observed under a microscope. Since all cell containing flow was directed through the cell trapping unit and the width of the channel at the protruding structure within the trapping unit ($5\ \mu\text{m}$) is smaller than the average diameter of MCF-7 cells ($18\pm 2\ \mu\text{m}$)³², single cells were immobilized in the trap.

Once a single cell was trapped, the upstream control valve (Fig. 1B) was activated while the cell washing outlet was opened to direct (the potentially cell-containing) carrier fluid to the cell trapping outlet. On average, 1.5 cells were introduced into the device per second. Single cells were consistently trapped in the microchip in 150 seconds or less. A lysis solution (100 mM Tris-HCl, pH 7.5, 500 mM LiCl, 10 mM EDTA, 1% LiDS, 5 mM dithiothreitol) was used to chemically lyse the trapped cells. By mixing oligo(dT)₂₅ beads with the cell lysate, mRNA templates from a single cell were captured and purified on bead surfaces.

Then, the beads were moved back to reaction chamber and retained by an external magnet. With the cell trapping and washing outlets closed and the upstream and downstream valves open (Fig. 1B), RT reagent was pipetted into the device chamber, followed by the closure of all the inlets and outlets. Then a pulsed temperature RT protocol was carried out (10 min at 25 °C and 50 min at 42 °C). Similarly, after RT, the PCR reagent was introduced into the device which simultaneously flushes away the RT reagent while the chip was situated on a magnet to immobilize the beads. Once PCR reagent completely filled the reaction chamber, all the outlets were sealed with plugs. Then the platform was placed on the stage of a fluorescent microscope. Each PCR process was initialized and thermocycled with the

following protocols: 10 min at 95 °C, followed by 35 cycles of 15 s at 95 °C and 1 min at 60 °C. The whole operation process is shown in Fig. 1C.

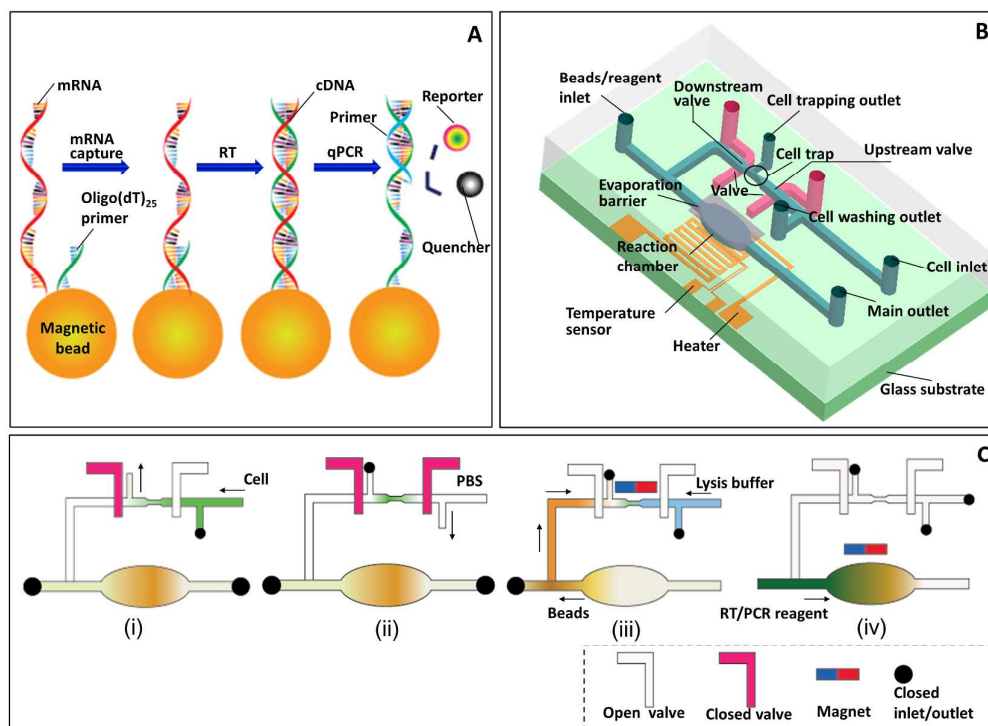


Figure 1. The microfluidic RT-qPCR device: (A) Bead-based RT-qPCR principle. Oligo(dT)₂₅ bead ($2.8 \pm 0.2 \mu\text{m}$) is composed of a superparamagnetic particle and a polymer shell. The bead can specifically target and capture mRNA molecules from virtually any crude sample and eliminate the need to purify total RNA when the desired information-bearing nucleic acid is mRNA. (B) Schematic of the device. (C) Operation of the device.

2.4 Microfluidic Device Fabrication

The RT-qPCR chip was fabricated using standard multi-layer soft lithography microfabrication techniques. Chrome (10 nm) and gold (100 nm) thin films were deposited and patterned onto a glass slide (Fisher HealthCare, Houston, TX) followed by passivation. AZ 4620 photoresist (Clariant Corp., Branchburg, NJ) was first spun

coated and patterned. Once developed, the photoresist was heated up to 200 °C for 1 h, which is above the glass transition temperature of the photoresist. Thus, the reflowing of the photoresist forms channels with a rounded cross section. Then, on the same wafer, SU-8 photoresist (MicroChem Corp., Newton, MA) was spun coated and patterned to define the other parts of the flow layer mold. In parallel, the mold for the pneumatic control layer was fabricated from SU-8 and measured using a Dektak 3 profilometer. Then, PDMS (Dow Corning) was poured over the molds and an additional vapor barrier was embedded in the flow layer PDMS. Sheets bearing the microfluidic features were then peeled off the mold followed by inlet and outlet hole punching. Also, uncured PDMS was spun on a wafer to form a featureless membrane (20 μm in thickness). The membrane was then sandwiched between the flow and control layer by oxygen plasma. Finally, the PDMS device was bonded to the heater and sensor by oxygen plasma resulting in a packaged device. The details of the fabrication process are shown in Fig. SI-1.

2.5 Experimental Set-up

Closed-loop temperature control of the device chambers was achieved using the integrated temperature sensor and heater with a proportional-integral-derivative (PID) algorithm implemented in a LabVIEW (National Instruments Corp., TX) program on a personal computer. The resistance of the sensor was measured by a digital multimeter (34420A, Agilent Technologies Inc., CA), and the heater was connected to a DC power supply (E3631, Agilent Technologies Inc., CA). The microfluidic valves of the device were controlled by individual pressure regulators (Concoa, Virginia Beach, Virginia) interfaced *via* 20 gauge stainless steel tubing (BD, Franklin Lakes, NJ) and Tygon tubing (ID: 0.79 mm, OD: 2.38 mm, Saint-Gobain, Grand Island, NY). The inlets and

outlets of the device were sealed off by polycarbonate plugs. The fluorescent intensity of the reaction was measured from images acquired by an inverted epifluorescence microscope (IX81, Olympus, Center Valley, PA) with a CCD camera (c8484, Hamamatsu, Boston, MA) of the reaction chamber. The schematic of the experimental set-up is shown in Fig. 2.

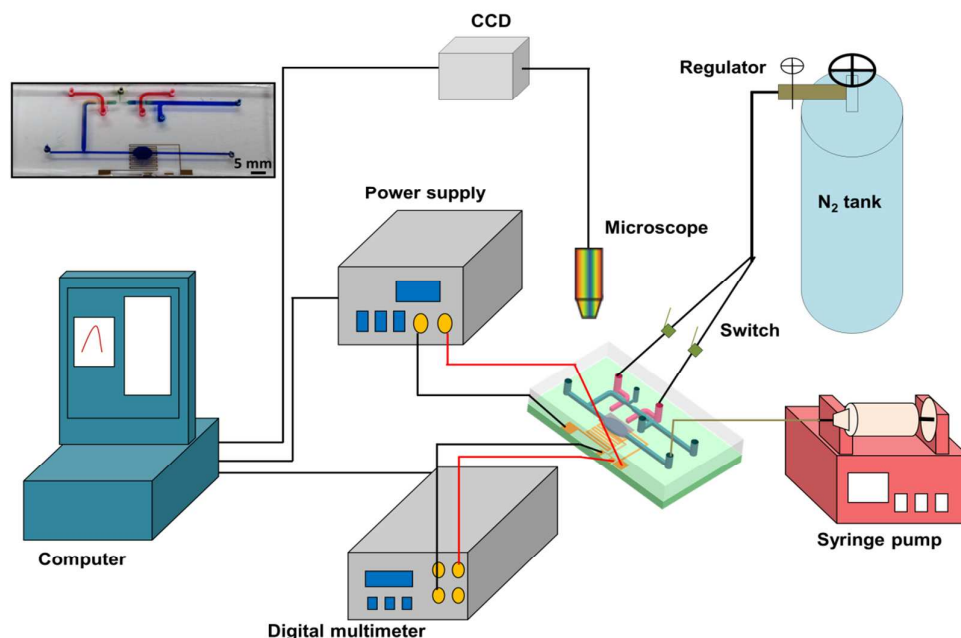


Figure 2. Schematic of the experimental set-up with a photograph of a packaged device in the inset.

2.6 Materials

MCF-7 cell lines were obtained from the American Type Culture Collection (ATCC, Manassas, VA). The Minimum Essential Medium (MEM), fetal bovine serum (FBS), penicillin-streptomycin (P/S, penicillin 10^4 unit/mL, streptomycin 10^4 mg/mL), 0.25% Trypsin-Ethylenediaminetetraacetic acid (EDTA), Dulbecco's phosphate-buffered saline (D-PBS), Vybrant multicolor cell-labeling kit (DiI, DiO and DiD), Dynabeads® mRNA Kit, TaqMan® reverse transcription reagents, oligo(dT)₁₆

(50 μ M) primer, CDKN1A primer/probe set (product number: Hs99999142_m1), XenoRNA control (10^5 copies/ μ L), TaqMan® Gene Expression master mix, thin-walled RNase-free PCR Tubes (0.2 mL), RNase-free water, RNaseZap Wipes, and MicroAmp® optical adhesive film for the evaporation barrier were purchased from Thermo Fisher Scientific Inc. (Grand Island, NY). Methyl methanesulfonate (~99%) and bovine serum albumin (BSA, $\geq 98\%$) were obtained from Sigma-Aldrich (St. Louis, MO).

3. Results and Discussion

In the experiments, we first performed on-chip thermal control characterization and microscope imaging calibration (Supplementary Information), as well as the influence of bead quantity, cell trapping, cell lysis, mRNA capture, and on-chip RT-PCR in the microchamber. We then demonstrated gene expression analysis through RT-qPCR of MMS treated and untreated single cells.

3.1 On-chip Experimental Validation

A hydrolysis primer/probe set and 2×10^4 copies XenoRNA were used to demonstrate the feasibility of on-chip RT-PCR. XenoRNA templates were reverse transcribed and amplified *via* 35 cycles of PCR. The amplification was compared with the no-template control (NTC). The protocol of the test is shown in Table SI-1. The fluorescent images and background subtracted fluorescent intensity are shown in Fig. 3A. For the on-chip RT-PCR of 2×10^4 copies XenoRNA, the fluorescent image of reporter showed much greater fluorescent intensity than the NTC sample. The mean fluorescent intensity value of three XenoRNA samples after 35-cycles of PCR was

2.7±0.2 compared to 0±0.05 with the NTC. This indicates there was a significant amplification of XenoRNA templates and negligible amplification of the NTC. Furthermore the consistent fluorescent intensity indicates that the reagent concentrations were stable during on-chip RT-PCR. Thus, we can conclude that the reagent absorption and evaporation during the thermal cycling process were effectively inhibited.

3.2 Optimization of Bead Volume Fraction in the Microchamber

We performed the optimization of the number of magnetic microbeads in the microchamber. With the microchamber containing varying numbers (from 7.5×10^5 to 7.5×10^6) of beads, XenoRNA templates (10^5 copies), approximately representing the amount of mRNA contained in a single cell) were amplified on the chip *via* 35 cycles of RT-PCR and detected by hydrolysis probes. The fluorescent intensity of the beads was measured at the end of the 35-cycle RT-PCR process for each bead quantity (Fig. 3B). The testing protocol is shown in Table SI-2. The fluorescence intensity, and hence the PCR reaction yield, initially increased with the number of beads in the chamber, reaching a maximum value at 3.75×10^6 beads, and then decreased as the bead quantity further increased. According to manufacturer-supplied information on the XenoRNA capture capacity of oligo(dT)₂₅ functionalized beads, the optimum bead quantity (3.75×10^6) is the number of beads approximately required to capture all the 10^5 copies XenoRNA. Thus, the initial increase in the PCR reaction yield reflected more mRNA being captured on the increasing number of beads. When the bead quantity exceeded the optimal value and further increased, it is likely that no additional copies of XenoRNA were captured in the chamber, while the decreasing net reaction volume in the chamber (with 3.75×10^6 and 7.5×10^6 beads occupying

roughly 9% and 19% of the chamber volume, respectively) caused a decrease in the reaction yield and the resulting fluorescence intensity. In subsequent RT-qPCR experiments in our device, we used this optimum bead quantity for experiments involving single cells, each of which was estimated to contain 10^5 - 10^6 copies of mRNA¹⁰.

3.3 On-chip mRNA Capture Efficiency Testing

Using the same primers (oligo(dT)₂₅), we performed experiments to assess bead-based mRNA capture efficiency. Different copy numbers of XenoRNA samples (10^4 , 2×10^4 , 5×10^4 and 10^5) were captured by 3.75×10^6 beads and the effluents were transferred to micro tubes and mixed with another bead solution including 3.75×10^6 beads with bound oligo(dT)₂₅ primers. RT-qPCR was then performed. The protocol for this experiment is shown in Table SI-3. Under these conditions the same primers were used allowing for direct comparison of the binding effluent and positive control qPCR. The results are shown in Fig. 3C. The value of ΔR_n , indicating the magnitude of the fluorescent signals and therefore amplification generated by PCR, was 2.9 for positive control (PC, 10^5 XenoRNA with 3.75×10^6 beads) after 40 cycles of PCR (Fig. 3C). While for the effluents the ΔR_n values remained below the threshold. Thus, we can conclude that after bonding, all the XenoRNA were captured by 3.75×10^6 beads and an undetectable amount of free RNA templates were residual in the binding waste. In addition, the lack of amplified products in the effluent verified that there was no significant bead loss as the chamber was flushed with buffer.

3.4 PCR Efficiency, Sensitivity and Repeatability

Similarly, to test the PCR efficiency, sensitivity and repeatability of our

microfluidic approach, we performed on-chip RT-qPCR using known copies of XenoRNA and compared the results to in-tube bead-based and solution-phase RT-qPCR performed under identical experimental conditions (Fig. 3D). The details of the procedure are shown in Table SI-4. For on-chip RT-qPCR, the mean C_q values with 10^4 , 2×10^4 , 5×10^4 and 10^5 copies XenoRNA were 29.7, 28.7, 27.3 and 26.4 respectively. The corresponding in-tube bead-based C_q values were 34.3, 33.9, 32.3 and 31.2 and the solution-phase C_q values were 33.7, 32.6, 31.1 and 29.9 respectively. Thus, the on-chip reactions had much lower mean C_q values than in-tube reactions, suggesting a more sensitive amplification process in the microfluidic device under the given experimental conditions. Additionally, we evaluated the PCR efficiency defined by $(10^{-1/k} - 1) \times 100\%$, where k is the slope of the C_q as a function of the logarithm of the template copy number (Fig. 3D)³³. We found that under the given experimental conditions, the PCR efficiency for the on-chip bead-based PCR testing (99.7%) was considerably higher than those for in-tube bead-based PCR (80.2%) and in-tube solution-phase PCR (83.9%). This improved efficiency for on-chip PCR was likely attributable to more efficient molecular interactions in the microscale reaction environment^{18-24, 31, 32}.

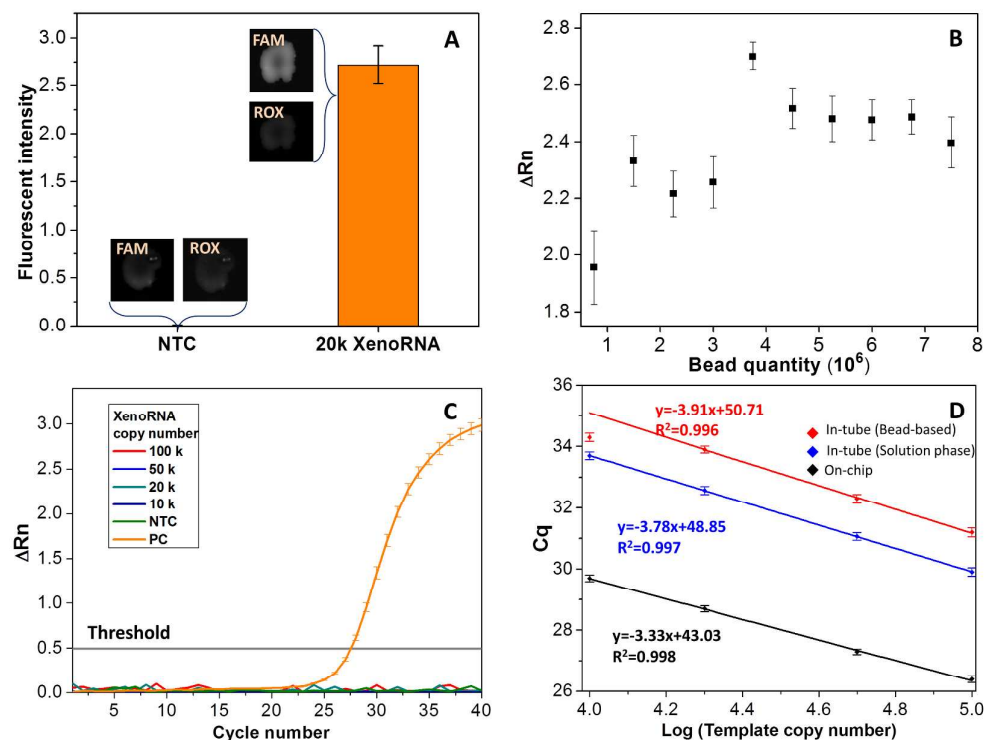


Figure 3. Bead based PCR optimization. (A) Validation of on-chip RT-qPCR. (B) Bead quantity analysis. 3.75×10^6 oligo(dT)₂₅ beads trapped 10^5 XenorNA copies most efficiently. (C) Quantified detection of mRNA trapping efficiency using 3.75×10^6 beads. There was no residual XenorNA template in the binding waste. (D) Mean and standard deviation of on-chip and in-tube RT-qPCR (with the C_q value at the 10,000 XenorNA copy number determined to be beyond the imaging system's measurement range and hence omitted from the linear fit). Error bars in the above figures were obtained from triplicates of experiments.

3.5 Single-Cell Isolation and Lysis

First, we investigated the single-cell trapping efficiency of the approach. The volume ratio of Vybrant dye and cell suspension (10^6 cell/mL) was 1:200. Using different carrier flow velocities, cells were dispensed at a fixed cell density and

transported to the trapping region. The relationship between the flow rate of cell suspension and the ability of the trap to immobilize a single cell was analyzed (Fig. 4).

To assess the probability of a single cell being trapped in the device, we conducted repeated experiments, in each of which a dilute cell suspension (10^5 cells/mL) was introduced into the device for cell trapping (Fig. 4A). The ratio of the number of experiments in which a single cell was successfully trapped to the total number of experiments provided a measure of cell trapping probability. Higher flow rates were found to cause a lower trapping probability as cells tended to pass through the trap because of the increased stress caused by the flow (Fig. 4B)³⁴. However, a lower flow rate would require a longer trapping time, or the time from the start of cell dispensing to the instant when a single cell was trapped, which could potentially impair the cell activity. To assess the combination of these effects, we defined a normalized trapping efficiency by $\varepsilon = C\rho/t$, where ρ is the trapping probability, t is the trapping time, and the scaling factor $C = (t/\rho)_{max}$ is the maximum of the ratio t/ρ calculated from the measurements. This parameter, obtained at flow rates ranging from 5 to 30 nL/s, was found to increase with the flow rate until reaching the 100% maximum at 15 nL/s, and then decreased as the flow rate further increased (Fig. 4C). Therefore, the optimum flow rate of 15 nL/s for cell suspensions 10^5 cells/mL in concentration was used in all subsequent single-cell gene expression analysis experiments.

We then studied the effects of cell lysis time on single-cell RT-qPCR. Single cells were trapped on-chip and incubated in lysis buffer (RNase proof) for different lengths of time, while microbeads preloaded in reaction chamber were transferred to the cell trapping unit, now containing cell lysate, by movement of an external magnet.

After incubation, the beads were moved back to the reaction chamber, and on-chip two-step RT-PCR was carried out to amplify the bead-bound mRNA templates and the reaction yield was analyzed (Fig. 4D). When cells were exposed to lysis buffer for less than 5 min, the end-point fluorescent intensity of RT-PCR increased with increasing time. However, at lysis times longer than 5 minutes, the signal decreased with increasing time. For short lysis times, the mRNA release process was incomplete. Extending the lysis time can increase the amount of mRNA released and the RT efficiency until enough time has passed where all mRNA have been released. Further increasing lysis duration can cause mRNA damage by RNase as the activity of the RNase inhibitor can be affected by oxidation. Thus, in the following experiments, we chemically lysed the trapped single cells for 5 min.

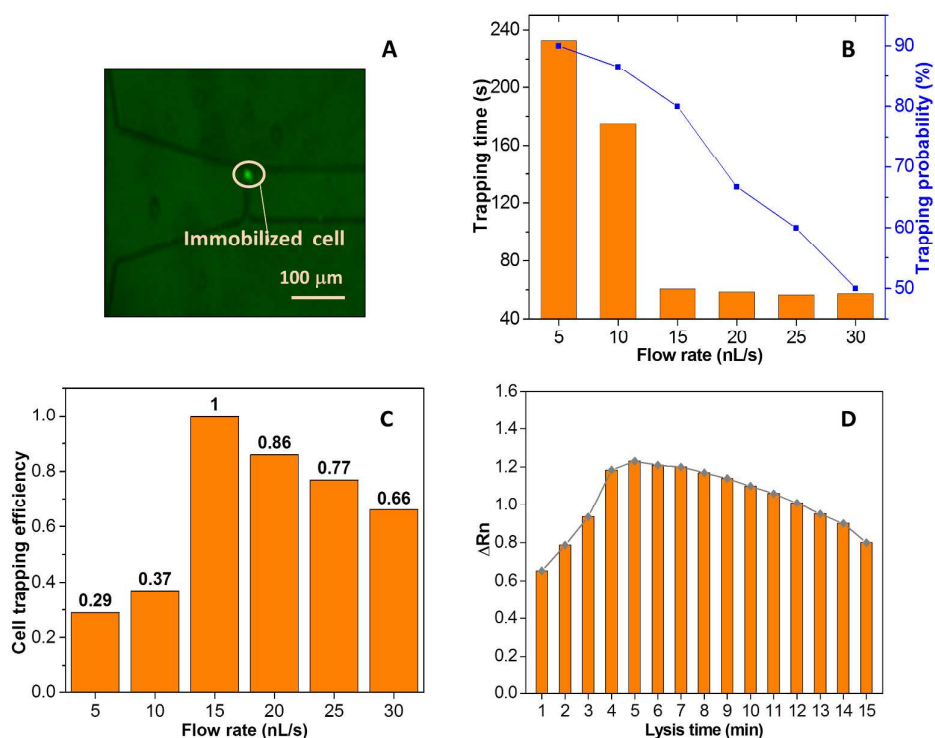


Figure 4. Testing of single-cell trapping and lysis. (A) Micrographs of single-cell trapping. (B) Flow rate effect on cell trapping time and probability. Trapping time and

probability decrease with increased flow rates. (C) Single-cell trapping efficiency. Maximum trapping efficiency obtained at a flow rate of 15 nL/s and a cell density of 10^5 cells/mL. (D) Lysis efficiency. The PCR output was highest for cells chemically lysed for 5 min.

3.6 Fully Integrated Single-Cell Gene Expression Profiling

All steps of single-cell RT-qPCR were integrated in our device. We detected chemically induced alterations in single-cell gene expression of MCF-7 cells treated with MMS. The gene expressions of single cells were assayed for the induction of CDKN1A using a hydrolysis probe/primer.

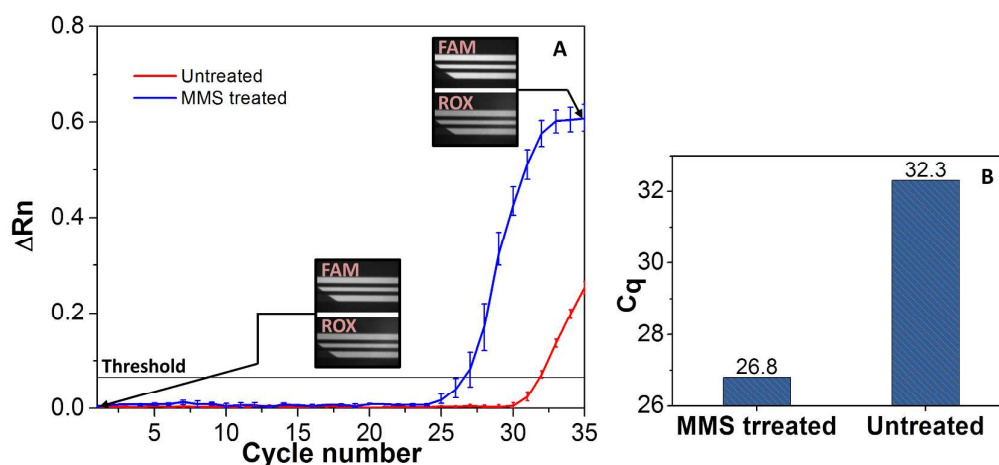


Figure 5. Fully integrated on-chip single-cell RT-qPCR. (A) Amplification curves of MMS treated (blue) and untreated (red) single-cell RT-qPCR. The points and error bars correspond to mean and standard deviation of fluorescent intensity during qPCR based on five repeated experiments. (B) Mean C_q values for integrated RT-qPCR in treated and untreated single cells were obtained from five repeated tests. The C_q values shown in Figure 5 indicate the approach was capable of detecting the MMS upregulation of CDKN1A gene expression at the single-cell level.

The amplification of the CDKN1A gene is shown in Fig. 5A. The threshold was calculated to be 0.07. For untreated (red line) and MMS treated single cells (blue line), the C_q values were 32.3 and 26.8 (Fig. 5B). The standard deviations of ΔR_n during the whole 35-cycle qPCR were below 0.04 and 0.01 for treated and untreated single cells respectively. Furthermore, the fluorescent images of the device at the first cycle and the 35th cycle of PCR indicated there was significant amplification of the CDKN1A gene in the reaction chamber. The ROX intensity detected during the entire RT-qPCR process was presented in Figure SI-6. The fluorescent intensity testing of no-template control was demonstrated in Figure SI-7.

Encoding by the CDKN1A gene which is located on chromosome 6 (6p21.2), p21/WAF1 can bind to and inhibit CDK activity, preventing phosphorylation of critical cyclin-dependent kinase substrates and blocking cell cycle progression³⁵. In our fully integrated single-cell gene expression profiling, the mean C_q value of MMS treated single MCF-7 cells was 5.48 cycles lower than the value for untreated single cells. Thus, the amount of starting templates in 2.5 h MMS treated MCF-7 cells was about 45 folds higher than in untreated single MCF-7 cells. After the MMS treatment, the transcript levels of the CDKN1A gene had been upregulated significantly and detected in our microchip. The results demonstrated the utility of our approach for potentially enabling rapid, sensitive and reliable single-cell gene expression analysis.

Conclusions

In this work, we have developed a bead-based microfluidic approach for integrated RT-qPCR at the single cell level. We first tested the mRNA capture efficiency and capacity of the bead, and evaluated the efficiency, sensitivity and repeatability of on-chip bead-based PCR in the microdevice. Then, the on-chip cell

trapping and lysis efficiencies were studied. To demonstrate the utility of the approach, we tested the gene expression levels of MMS treated and untreated single MCF-7 cells using our approach. The experimental results showed that the PCR efficiency and the sensitivity of RT-qPCR can be significantly enhanced by using our integrated approach. We also showed that our approach is capable of detecting the expression of CDKN1A gene upregulated by MMS treatment within 27 cycles at the single cell level. These results demonstrated the utility of our approach for potentially enabling rapid, sensitive and reliable single-cell gene expression analysis. In future work, we will extend this approach to construct a microfluidic array that will allow parallelized and multiplexed single-cell RT-qPCR, which will ultimately enable high-throughput single-cell gene expression analysis in basic biological research and clinical diagnostics.

Acknowledgements

We gratefully acknowledge financial support from the National Institutes of Health (Award Nos. 5U19 AI067773 and 8R21GM104204). The authors would like to thank Dr. Jung-Chi Liao for granting access to an Olympus IX 81 fluorescent microscope, and Dr. Lubomir Smilenov for the help in using an Applied Biosystems 7900HT Fast Real-Time PCR system. H.S. also appreciates a National Scholarship from the China Scholarship Council.

References

1. Q. F. Wills, K. J. Livak, A. J. Tipping, A. J. Tipping, T. Enver, A. J. Goldson, D. W. Sexton, C. Holmes, *Nature Biotechnology*, 2013, **31**, 748-752.
2. R. Sandberg, *Nature Methods*, 2014, **11**, 22-24.
3. K.H. Narsinh, N. Sun, V. Sanchez-Freire, A.S. Lee, P. Almeida, et al., *Journal of Clinical Investigation*, 2011, **121**, 1217-1221.
4. D. W. M. Tan, K.B. Jensen, M.W.B. Trotter, J.T. Connelly, S. Broad, F. M. Watt, *Development*, 2013, **140**, 1433-1444.
5. C. Trapnell, D. Cacchiarelli, J. Grimsby, P. Pokharel, S. Li, M. Morse, N.J. Lennon, K. J. Livak, T. S. Mikkelsen, J. L. Rinn, *Nature Biotechnology*, 2014, **32**, 381-386.
6. V. Moignard, I. C. Macaulay, G. Swiers, F. Buettner, J. Schütte, et al., *Nature cell Biology*, 2013, **15**, 363-372.
7. S. Picelli, Å. K. Björklund, O. R. Faridani, et al., *Nature Methods*, 2013, **10**, 1096-1098.
8. D. Lovatt, B. K. Ruble, J. Lee, et al., *Nature Methods*, 2014, **11**, 190-196.
9. S. Islam, A. Zeisel, S. Joost, et al., *Nature Methods*, 2013, **11**, 163-166.
10. J. H. Lee, E. R. Daugharthy, J. Scheiman, et al., *Science*, 2014, **343**, 1360-1363.
11. R. A. Beckman, G. S. Schemmann, C. H. Yeang, *Proceedings of the National Academy of Sciences*, 2012, **109**, 14586-14591.
12. J. M. Spaethling, J. H. Eberwine, *Current Opinion in Pharmacology*, 2013, **13**, 786-790.
13. S. Cao, J. Han, J. Wu, et al., *BMC Genomics*, 2014, **15**, 4.
14. X. Adiconis, D. Borges-Rivera, R. Satij, et al., *Nature Methods*, 2013, **10**, 623-629.
15. V. Sanchez-Freire, A. D. Ebert, T. Kalisky, et al., *Nature Protocols*, 2012, **7**, 829-838.
16. D. Ramsköld, S. Luo, Y. C. Wang, et al., *Nature Biotechnology*, 2012, **30**, 777-782.
17. M.G. Carter, A.A. Sharov, V. VanBuren, D.B. Dudekula, C.E. Carmack, C. Nelson, et al., *Genome Biology*, 2005, **6**, R61.
18. D. Mark, S. Haerberle, G. Roth, F. von Stetten, R. Zengerle, *Chemical Society Reviews*, 2010, **39**, 1153-1182.
19. G. Jiang, D. J. Harrison, *Analyst*, 2000, **125**, 2176-2179.
20. J. W. Hong, V. Studer, G. Hang, et al., *Nature Biotechnology*, 2004, **22**, 435-439.
21. J. S. Marcus, W. F. Anderson, S. R. Quake., *Analytical Chemistry*, 2006, **78**, 3084-3089.
22. N. Bontoux, L. Dauphinot, T. Vitalis, et al., *Lab on a Chip*, 2008, **8**, 443-450.
23. N. M. Toriello, E. S. Douglas, N. Thaitrong, et al., *Proceedings of the National Academy of Sciences*, 2008, **105**, 20173-20178.
24. R. N. Zare, S. Kim., *Annual Review of Biomedical Engineering*, 2010, **12**, 187-201.
25. J. Avesar, T. B. Arye, S. Levenberg., *Lab on a Chip*, 2014, **14**, 2161-2167.
26. T. Matsunaga, M. Hosokawa, A. Arakaki, T. Taguchi, T. Mori, T. Tanaka, et al., *Analytical Chemistry*, 2008, **80**, 5139-5145.
27. T. Nolan, R.E. Hands, S.A. Bustin, *Nature Protocols*, 2006, **1**, 1559-1582.
28. S. A. Bustin, V. Benes, J. A. Garson, et al., *Clinical Chemistry*, 2009, **55**, 611-622.
29. D.C. Saunders, G.L. Holst, C.R. Phaneuf, N. Pak, M. Marchese, N. Sondej, et al., *Biosensors and Bioelectronics*, 2013, **44**, 222-228.
30. A.K. White, M. VanInsberghe, O.I. Petriv, M. Hamidi, D. Sikorski, M.A. Marra, et al., *Proceedings of the National Academy of Sciences*, 2011, **108**, 13999-14004.

31. R. M. Clegg, *Current Opinion in Biotechnology*, 1995, **6**, 103-110.
32. S.K. Arya, K.C. Lee, D. Bin Dah'alan, Daniel, A.R.A. Rahman, *Lab on a Chip*, 2012, **12**, 2362-2368.
33. C. Ramakers, J. M. Ruijter, R. H. L. DePrez, et al., *Neuroscience Letters*, 2003, **339**, 62-66.
34. I. Kumano, K. Hosoda, H. Suzuki, et al., *Lab on a Chip*, 2012, **12**, 3451-3457.
35. T. Abbas, A. Dutta , *Nature Reviews Cancer.*, 2009, **9**, 400-414.